24th ASME Wind Energy Symposium
in conjunction with the 43rd AIAA Aerospace Sciences Meeting & Exhibit
AIAA-2005-1459

Low-Dimensional Representations of Wind Turbine Inflow Turbulence and Response using Proper Orthogonal Decomposition

Korn Saranyasoontorn* and Lance Manuel†
Department of Civil Engineering, University of Texas at Austin, Austin, TX 78712

A demonstration of the use of Proper Orthogonal Decomposition (POD) is presented for the identification of energetic modes that characterize the spatial random field describing the turbulence experienced by a wind turbine. POD techniques are efficient because a limited number of such modes can often describe the preferred turbulence spatial patterns and they can be empirically developed using data from spatial arrays of sensed input/excitation. In this study, for demonstration purposes, rather than use field data, POD modes are derived by employing the covariance matrix estimated from simulations of the spatial inflow turbulence field based on a Kaimal spectral model. The efficiency of the method in deriving reduced-order representations of the along-wind turbulence field is investigated by studying the rate of convergence (to total energy in the turbulence field) that results from the use of different numbers of POD modes, and by comparing the frequency content of reconstructed fields derived from the modes. The National Wind Technology Center's Advanced Research Turbine (ART) is employed in the examples presented where both inflow turbulence and turbine response are studied with low-order representations based on a limited number of inflow POD modes. Results suggest that a small number of energetic modes can recover the low-frequency energy in the inflow turbulence field as well as in the turbine response measures studied. At higher frequencies, a larger number of modes is required to accurately describe the inflow turbulence. Blade turbine response variance and extremes, however, can be approximated by a comparably smaller number of modes due to diminished influence of higher frequencies.

I. Introduction

PROPER Orthogonal Decomposition (POD) is a powerful numerical technique that is often used to extract preferred spatial "modes" or patterns of variations in a high-dimensional random field by using measured data. Mathematically, POD procedures empirically identify deterministic orthogonal basis functions (modes) that preserve the energy of fluctuations and the spatial coherence in the random field in an efficient manner. An appealing feature of the method is that it provides an optimal representation of the stochastic field compared to other linear orthogonal decomposition techniques, and is thus suited for use in deriving low-dimensional descriptions of complex random fields. By truncation of the higher modes that are associated with lower energy levels, efficient computational schemes result that can describe the random field with accuracy.

POD techniques have been widely used in many engineering applications – for example, in turbulent fluid flows,[1] wind engineering,[2,3] and studies related to turbulence and atmospheric stability for wind turbines.[4] The effectiveness of these techniques in describing dominant features of a high-dimensional random field as illustrated in such studies suggests possible benefits that could result from their use in characterizing the inflow turbulence field experienced by wind turbines. Such characterizations can be useful in the analysis of wind turbine loads. Also, once the inflow turbulence modes at a site have been empirically identified using POD techniques, it is possible that only a few such modes associated with high energy might suffice for accurate description of the spatial inflow turbulence structure. Moreover, it is possible that an even smaller number of these estimated inflow POD modes

* Graduate Research Assistant, AIAA Student Member.
† Assistant Professor.

may be required to derive an accurate representation of the turbine loads, due to filtering effects of the structural and aerodynamic system that can render some POD modes insignificant. Finally, POD techniques can be useful in assessing which inflow characteristics most significantly drive turbine loads by investigating the response measures and loads that result from the use of different subsets of inflow POD modes.

In this preliminary study, the effectiveness of the POD procedure in identification of key spatial patterns in the inflow turbulence is of interest for the 600-kW Advanced Research Turbine (ART) that is part of an ongoing research program at the National Wind Technology Center (NWTC). We employ simulation studies of the three-dimensional inflow turbulence field influencing the rotor. Ordinarily, all three turbulence components need to be part of the decomposition procedure that we describe. However, the coherence at all frequencies and separations of the across-wind and vertical turbulence components is assumed to be zero. The cross-coherence between any orthogonal turbulence components is also assumed to be zero. Hence, only decomposition of the along-wind inflow turbulence component needs to be considered in the POD procedure. It is important to note that the POD technique demonstrated for the along-wind turbulence component alone can easily be extended to characterize the full three-dimensional inflow field in which non-zero coherence in each turbulence component and non-zero cross-coherence among each pair of orthogonal components is included. In our illustrations here, the POD technique is employed for the along-wind turbulence component; the (uncoupled) across-wind and vertical turbulence components are still included in that the power spectral density functions for these components at all spatial locations are used to simulate non-coherent time series for these components.

We begin with a brief review of the theoretical framework for POD analysis. The effectiveness of the method will be assessed by studying the energy of empirically derived orthogonal (and uncorrelated) sub-processes of a inflow field simulated based on the Kaimal spectral model and the IEC exponential coherence model, recommended in the IEC guidelines[5] for wind turbine design (see the appendix for details about these models). The accuracy of reduced-order inflow representations using a limited number of POD modes to describe the target along-wind turbulence field is studied. The frequency content of the original turbulence field and that of its low-dimensional representation are also compared. To evaluate the efficiency of the POD procedure in characterizing wind turbine response, we employ reconstructed inflow fields based on different numbers of POD modes as input to a wind turbine response simulator. Statistics of various turbine response measures are estimated from the time series that use a reduced-order response representation and these are compared with the original (target) response time series.

II. Proper Orthogonal Decomposition

In the following, we present the key concepts upon which Proper Orthogonal Decomposition is based. Several references related to these techniques can be found in the literature (see, for example, Ref. 1,2).

In one form of Proper Orthogonal Decomposition, called in some places Covariance Proper Transformation (CPT), assume that one is given N weakly stationary zero-mean correlated random processes $\boldsymbol{V}(t) = \{V_1(t), V_2(t), \ldots V_N(t)\}^T$ and a corresponding $N \times N$ covariance matrix, $\mathbf{C_V}$. It is possible to diagonalize $\mathbf{C_V}$ so as to obtain the (diagonal) matrix, $\boldsymbol{\Lambda}$.

$$\boldsymbol{\Phi}^T \cdot \mathbf{C_V} \cdot \boldsymbol{\Phi} = \boldsymbol{\Lambda}; \quad \mathbf{C_V} \cdot \boldsymbol{\Phi} = \boldsymbol{\Phi} \cdot \boldsymbol{\Lambda}; \quad \boldsymbol{\Lambda} = \mathrm{diag}\{\lambda_1, \lambda_2, \ldots \lambda_N\} \tag{1}$$

The eigenvectors, $\boldsymbol{\Phi} = \{\boldsymbol{\phi}_1, \boldsymbol{\phi}_2, \ldots \boldsymbol{\phi}_N\}$ of $\mathbf{C_V}$ describe basis functions in a principal space. It is now possible to rewrite the original N correlated processes, $\boldsymbol{V}(t)$, in terms of N uncorrelated *scalar* processes, $\boldsymbol{Z}(t) = \{Z_1(t), Z_2(t), \ldots Z_N(t)\}^T$ such that

$$\boldsymbol{V}(t) = \boldsymbol{\Phi} \cdot \boldsymbol{Z}(t) = \sum_{j=1}^{N} \boldsymbol{\phi}_j Z_j(t) \tag{2}$$

where the uncorrelated scalar processes can be derived by employing the orthogonality property,

$$\boldsymbol{Z}(t) = \boldsymbol{\Phi}^T \cdot \boldsymbol{V}(t) \tag{3}$$

The covariance matrix for $\boldsymbol{Z}(t)$, namely $\mathbf{C_Z}$, is equal to the diagonal matrix, $\boldsymbol{\Lambda}$, and an energy measure associated with each $Z_j(t)$ can be defined in terms of its variance, λ_j. The original random processes are conveniently decomposed into N uncorrelated random processes. If the eigenvalues, $\boldsymbol{\Lambda}$, are sorted in decreasing order, a reduced-order representation, $\hat{\boldsymbol{V}}(t)$, is obtained by only retaining the first M covariance-based POD modes as follows:

$$\hat{\boldsymbol{V}}(t) = \sum_{j=1}^{M} \boldsymbol{\phi}_j Z_j(t), \text{ where } M < N \tag{4}$$

Note that in the description above, $\boldsymbol{V}(t)$, can represent scalar wind speed (turbulence) random processes at N different locations defined for a single direction (such as along-wind), but it could also represent all three

components of turbulence at various locations. Clearly, an extension of the POD technique to model a three-dimensional turbulence field is straightforward, even though only along-wind turbulence is considered here.

An attractive feature of the POD procedure is that the derived low-dimensional representation of a weakly stationary Gaussian random process is optimal compared to any other linear orthogonal decomposition.[1,6,7] In the present study, CPT will be employed to decompose a simulated inflow turbulence random field as is discussed next.

III. Numerical Examples

In this section, the accuracy of reduced-order inflow turbulence representations based on covariance proper transformation (CPT) in describing the along-wind turbulence field as well as the structural response of a wind turbine is assessed. For the sake of illustration, 19 ten-minute simulations of a wind turbulence vector random field were generated with a sampling frequency of 20 Hz over the rotor plane of the National Wind Technology Center's Advanced Research Turbine (ART). This turbine, see Fig. 1, is a Westinghouse 600-kW, upwind, two-bladed teetered-hub turbine with a hub height of 36.6 m, a rotor diameter of 42 m, and a constant rotor speed of 42 rpm.[8] The computer program, SNwind,[9,10] was used for carrying out the three-dimensional inflow field simulation. The Kaimal spectral model and the IEC exponential coherence model recommended in the IEC guidelines[5] for wind turbine designs were assumed for the inflow simulation.

For the inflow field simulation, a 6×6 rectangular grid discretization of the rotor plane (with a vertical and lateral grid spacing of 42 m) with one additional point at the center of the rotor was used as shown in Fig. 2. Since only the along-wind turbulence component is considered in modeling the turbulence field, a total of 37 inflow turbulence POD modes can be defined to represent this field. In the following, we first discuss the accuracy of reduced-order representations of the simulated turbulence field.

Figure 1. The National Wind Technology Center's Advanced Research Turbine (ART) used in the numerical studies.

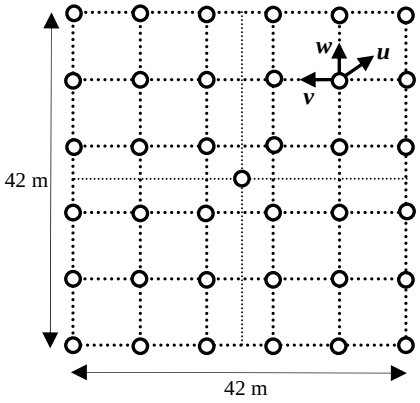

Figure 2. Thirty-seven spatial locations on the 42m×42m rotor plane of the ART machine used in the POD analyses.

A. POD Representation of the Inflow Turbulence Field

The along-wind inflow turbulence POD modes are empirically derived by employing covariance proper decomposition (CPT). A 37×37 sample covariance matrix is estimated from the 19 ten-minute simulations of the spatial inflow turbulence field. The eigenvalues, λ_j, associated with the energy of each POD mode are computed and shown in Fig. 3. Clearly, the first POD mode accounts for a considerably large contribution of the total energy compared with the energy from the other modes. Further, it is seen from the plot of the cumulative fraction of energy preserved in low-order representations of the along-wind turbulence field in Fig. 4 that the first mode alone carries approximately 65 percent of the total energy of the turbulence field while almost 80 percent of the total energy is captured by the first five POD modes. It should be mentioned here that reduced-order POD representations are especially efficient when the stochastic random field under consideration is strongly correlated over different spatial scales, which is the case for the along-wind turbulence component (this is why projections of the original field onto the very first few modes preserve a large proportion of the energy in along-wind turbulence.) The other two orthogonal turbulence components typically exhibit relatively weaker correlation;[11] hence, the usefulness of the POD procedure may be limited for these other turbulence components. The first four (out of 37) energetic eigenmodes of the simulated along-wind turbulence field are illustrated in Fig. 5. The energy (variance) corresponding to each POD mode, λ_j, is also indicated in the figure. It is clear from the figure that the first mode which accounts for the largest energy in the turbulence field

describes a mostly uniform spatial inflow pattern over the rotor plane, while the second and third modes (each with similar energy levels) describe sheared turbulence patterns in the lateral and vertical directions, respectively. As expected, the patterns of inflow turbulence in higher modes, such as the fourth mode shown in Fig. 4, become increasingly complex when compared with those of the first three modes.[12]

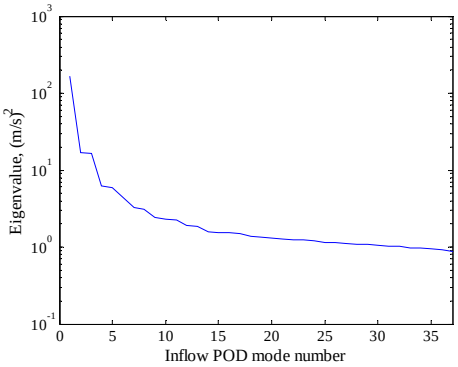

Figure 3. Eigenvalues of the covariance matrix of the along-wind turbulence for each POD mode.

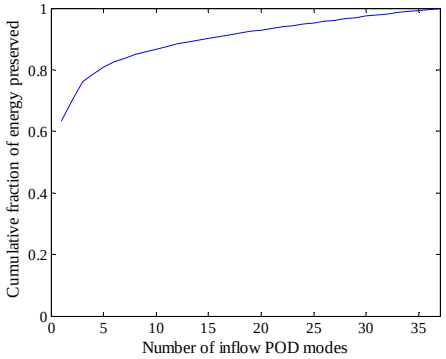

Figure 4. Cumulative fraction of energy in low-order representations of along-wind turbulence.

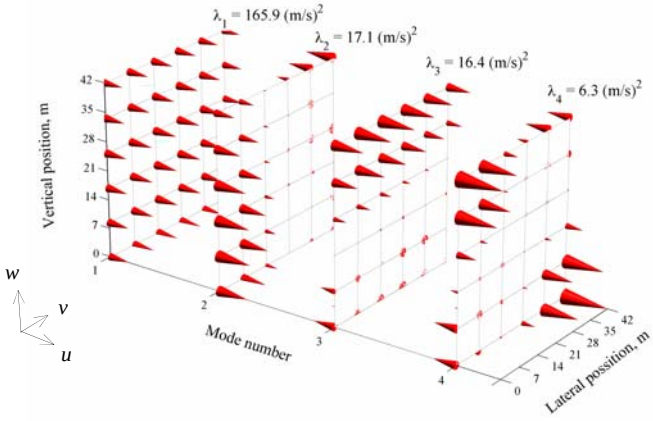

Figure 5. First four eigenmodes and corresponding eigenvalues of the covariance matrix of the along-wind turbulence field.

Convergence to the variance in the inflow turbulence at each spatial location over the rotor plane with different low-order representations (using 1, 5, and 10 POD modes) is demonstrated in Fig 6. It is found that the convergence rates at different locations are quite different. With the first mode alone, the variance of the along-wind turbulence at locations near the center of the rotor is closer to the target when compared with locations near the edge of the rotor plane. With an increase in the number of the POD modes included, the variance at all locations is estimated with similar levels of accuracy. This is because the eigenmodes beyond the first that describe spatial shear of the inflow turbulence and other non-uniform patterns (see Fig. 5) are needed, especially at locations away from the center. These results suggest that with the first few modes, the variance (or energy) of the reconstructed turbulence field is primarily concentrated near the rotor center; after a sufficient number of additional modes are included, the energy of the turbulence field tends to get more accurately represented at all locations on the rotor plane

Apart from the variance, the correlation in along-wind turbulence at different locations should be preserved with reasonable accuracy in low-dimensional representations of the full turbulence field. Figure 7 shows rates of convergence of correlation coefficients between the along-wind turbulence at the rotor center and that at each of the other 36 grid points. Note that when only one POD mode is employed, the correlation coefficients will be identically unity indicating perfect correlation in the single sub-process used for the turbulence at all locations. As the number of the POD modes employed increases, the correlation coefficients between center and any location systematically decrease and approach their target values. This happens because the POD procedure decomposes the original random processes into random sub-processes each of which is perfectly correlated at the different locations, but distinct element sub-processes (from each mode) are uncorrelated.

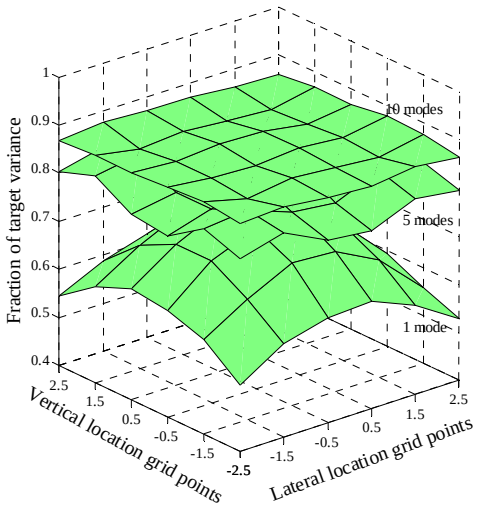

Figure 6. Fraction of the target variance of the along-wind turbulence component at the 36 grid points on the rotor plane (see Fig. 2) based on 1, 5, and 10 POD modes.

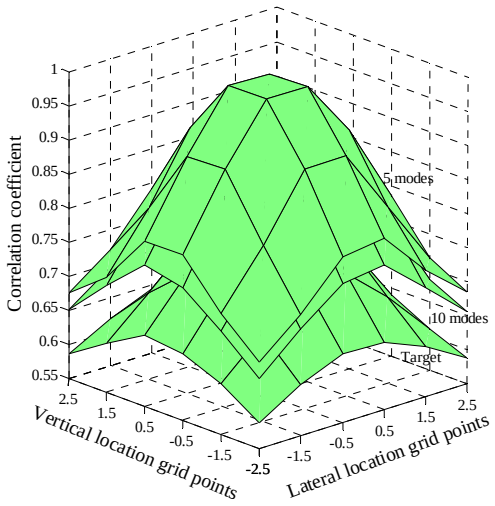

Figure 7. Correlation coefficients between the along-wind turbulence at hub center and that at each of the 36 grid points on the rotor plane (see Fig. 2) based on 5 and 10 POD modes compared with the target values.

Reconstructed time series of the along-wind turbulence at the center of the rotor plane based on 1, 5, and 10 inflow modes are plotted in Fig. 8 along with the target time series simulated using SNwind. Only a single 10-minute segment is shown here. It is seen that when a small number of POD modes is employed, the low-frequency characteristics in the inflow are captured quite accurately. To obtain a good representation of the high-frequency content, however, a larger number of POD modes is required. In order to study the frequency content of the reconstructed time series in greater detail, power spectral density functions (PSDs) from the 19 ten-minute turbulence time series at the center of the rotor plane were estimated and are shown in Fig. 9. The PSDs for the reconstructed time series were estimated based upon Welch's modified periodogram method using 50-percent overlapping segments, each multiplied by a Hanning data window. The Kaimal spectral model on which the full-field simulation is based is also shown for the sake of comparison. It is seen that the PSD of the SNwind-simulated time series matches the Kaimal model very well.

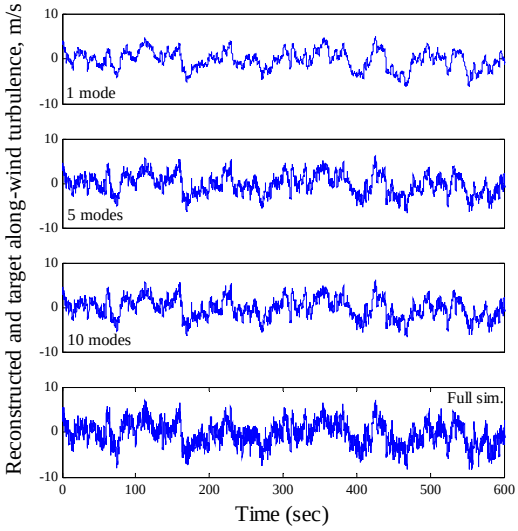

Figure 8. Reconstructed time series of the along-wind turbulence at the rotor center based on 1, 5, and 10 POD modes (compared with the target).

The plot confirms our statement that only a small number of POD modes are needed to accurately describe the low-frequency inflow energy while a much larger number may be required at higher frequencies. This is mainly because the turbulence field is more coherent at low frequencies as has been verified in many experimental results (see, for example, Refs. 11 and 13) and, hence, the efficiency of the POD procedure is more obvious in the low-frequency range. Note that no significant improvement in convergence to the target full-field simulation PSD at the rotor center resulted from increasing the number of included POD modes from 5 to 10. This can be explained, as was done while discussing Fig. 6, by the fact that the convergence rate of the energy in the inflow turbulence near the center is greatest when the first few POD modes are employed. As additional modes beyond these first few are included, improvement in total variance mainly improves inflow descriptions at locations towards the outer edges of the rotor plane while making only small incremental improvements to the energy (and, thus, the PSD) at locations near the center.

To ensure that employing a reduced-order POD representation of the along-wind turbulence field does not introduce large variability in the inflow turbulence, the median, 5th percentile, and 95th percentile of the PSD estimates from the 19 ten-minute reconstructed inflow turbulence time series at the center of the rotor plane based on 5 POD modes as well as similar PSD estimates based on full-field simulation are compared in Fig. 10. It is clear from the figure that the variability in PSD estimates at all frequencies is small with the 5 POD modes and, more importantly, the variability is comparable with that from full-field simulations. This suggests that employing the POD procedure to describe the along-wind turbulence field does not introduce additional variability to that present in the target turbulence random field approximated by the reduced-order POD representation.

Finally, we investigate coherence in along-wind turbulence as estimated by using reduced-order POD representations. Figures 11 and 12 show coherence spectra based on reconstructed time series data from 1, 5, and 10 POD modes for two different lateral separations of 8.4 and 16.8 meters. The target coherence spectrum based on the IEC exponential coherence model and the coherence spectrum based on full-field simulation are also included in the figures for the sake of comparison. It is seen that the coherence derived from a single POD mode is equal to unity at all frequencies indicating perfect correlation (due to the single sub-process used for all spatial locations) as was discussed before. It is seen that the first five POD modes are almost sufficient to describe the coherence at the larger separation of 16.8 meters. Over shorter separations, especially at higher frequencies, additional modes are necessary in order to reduce the overly large correlation that result when too few POD modes are included.

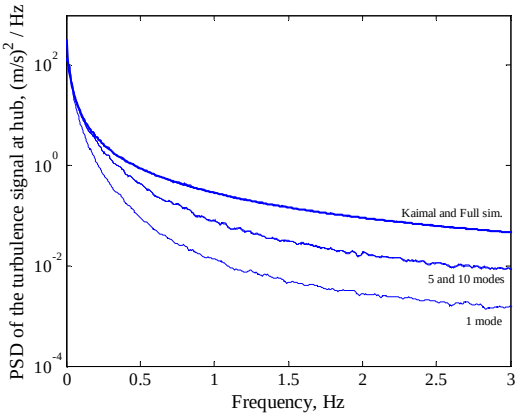

Figure 9. PSDs of the reconstructed along-wind turbulence at the rotor center using 1, 5, and 10 POD modes compared with the full-field simulation and the target Kaimal spectral model.

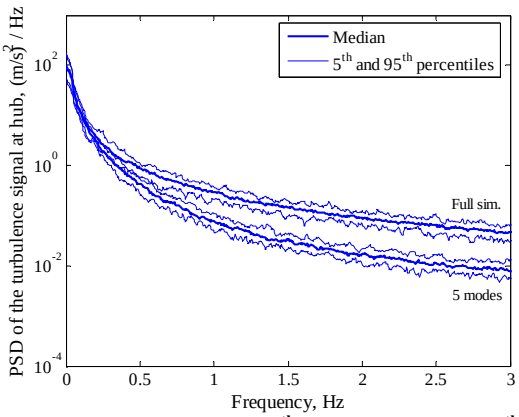

Figure 10. Median, 5th percentile, and 95th percentile PSD estimates of along-wind turbulence at the rotor center using 5 POD modes compared with similar estimates from full-field simulations.

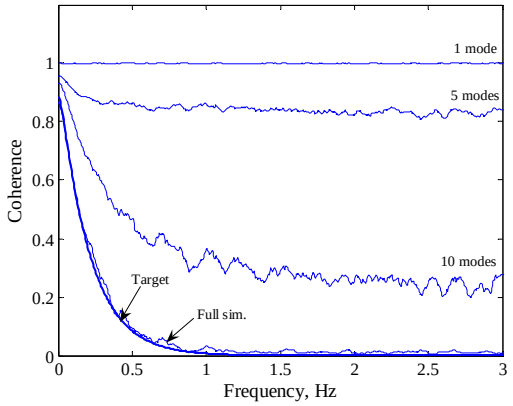

Figure 11. Coherence spectra of the reconstructed along-wind turbulence components at a lateral separation of 8.4 m using 1, 5, and 10 POD modes compared with the full-field simulation and the target IEC exponential coherence model.

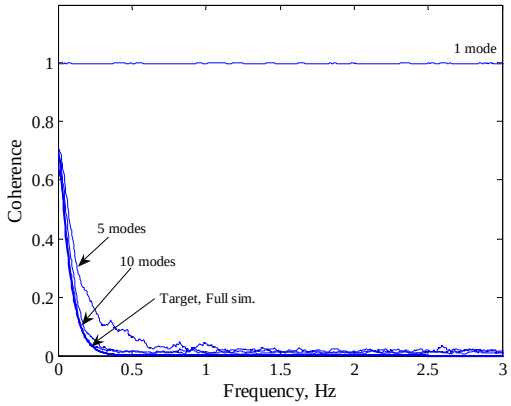

Figure 12. Coherence spectra of the reconstructed along-wind turbulence components at a lateral separation of 16.8 m using 1, 5, and 10 POD modes compared with the full-field simulation and the target IEC exponential coherence model.

B. Contribution of Inflow Modes on Turbulence Response

Reconstructed along-wind turbulence time series, with several choices for the retained number of empirical orthogonal modes, were used to perform wind turbine simulations. Though the other two orthogonal turbulence components (across-wind and vertical) were not considered in the POD analysis as was discussed earlier, the turbulence fields for these two components as obtained from the SNwind simulations were added to the reduced-order along-wind turbulence while carrying out the wind turbine simulation. Our intent here is to illustrate how low-dimensional representations of the turbulence field based on the POD procedure may be applied in wind turbine load analysis. We are interested in determining how much each inflow POD mode contributes to various wind turbine response measures or, equivalently, how many distinct inflow field patterns are required to accurately represent the turbine response characteristics. The computer program, FAST (Fatigue, Aerodynamics, Structures, and Turbulence),[14] was employed to carry out the wind turbine simulations. The input inflow data for FAST were based on the results from POD analyses for the 19 ten-minute simulated along-wind turbulence time series (along with the across-wind and vertical turbulence time series) resulting from SNwind runs. Our main interest is in the comparison of various turbine response statistical estimates based on different numbers of POD modes; these include estimates of the variance and ten-minute extremes of (i) flapwise bending moment at the blade root, (ii) edgewise bending moment at the blade root, and (iii) fore-aft base bending moment of the tower. These turbine response statistics are studied here because they are commonly considered in wind turbine design. To achieve good estimates of turbine response statistics, a large number of ten-minute time series are generally required. However, in this preliminary study, only 19 ten-minute inflow time series were used for illustration purposes.

Figure 13 shows plots of the first 200 seconds of the response time series (out of a total of 19×600 = 11400 seconds of available data) derived from using 1, 5, and 10 inflow POD modes as input to FAST in comparison with the target turbine response derived from the full-field inflow simulation. Zoomed-in response plots over a 10-second duration are plotted in Fig. 14 in order to emphasize the finer details in the original and the POD-based signals. As with the inflow turbulence time series, by visual inspection of Figs. 13 and 14, it can be seen that a few inflow POD modes are able to capture much of the low-frequency character of the target turbine response (at least for the blade bending response measures) but they miss the high-frequency content that might be of importance in wind turbine fatigue and extreme loads analysis. A larger number of inflow modes is required to describe the high-frequency response fluctuations. This is verified by studying the frequency content of the various response signals by means of power spectra in Figs. 15, 16, and 17, respectively, for flapwise bending moment at the blade root, edgewise bending moment at the blade root, and fore-aft tower bending moment at the base. It is clear from these figures that only a few inflow modes are needed to describe the low-frequency content in the turbine response. Peaks in the response spectra due to rotational sampling at 0.7 Hz (1P), 1.4 Hz (2P), 2.1 Hz (3P), etc. and due to the first fore-aft tower bending natural frequency (around 0.85 Hz) are approximated reasonably well by the reduced-order representations of the inflow turbulence. This is especially true for those peaks in the low-frequency region. A large portion of the energy (and variance) in the turbine loads studied is contributed by low frequencies; hence, only a small number of inflow POD modes may be required to derive an accurate representation of these turbine loads. For example, a single inflow POD mode appears to be adequate to represent the 1P peaks in the blade bending load spectra (see Figs. 15 and 16).

Similar to the investigation of the variability in PSD estimates of the inflow turbulence at the rotor center (Fig. 10), the median, 5^{th} percentile, and 95^{th} percentile PSD estimates from the 19 ten-minute flapwise blade bending moment time series based on 5 POD modes as well as on full-field inflow simulation are compared in Fig. 18. Variability in PSD estimates using 5 POD modes is seen to be small and comparable with that from full-field simulation, indicating that the POD procedure does not introduce additional variability in turbine response PSDs.

Estimates of mean values of the three turbine response measures derived using a few inflow POD modes were computed and compared with target values (from full-field inflow simulation). It was found that recovered mean values based on a single inflow POD mode closely matched the target mean values in all cases. The ratio of the approximate variance derived using 1, 5, 10, 20, and 37 inflow POD modes to the target variance for each of the turbine response measures is shown in Fig. 19. (Note that the variance is already explained in part by the PSD plots shown in Figs. 15, 16, and 17.) It can be seen that only a very few inflow modes are needed to capture most of the variance in the edgewise blade bending moment loads. Physically, this is because these edgewise blade bending loads depend primarily on the rotational speed of the turbine and on gravity loading due to the self-weight of the blade, and not very much on the wind loads. Another explanation is that a large proportion of energy for edgewise bending is concentrated in the low-frequency region and near the rotational frequency of 0.7 Hz (see Fig. 16) where a relatively small number of inflow POD modes can accurately describe the inflow turbulence field. The first inflow

POD mode alone accounts for approximately 95% of the edgewise blade bending moment variance. For the flapwise blade bending moment and the fore-aft tower bending moment, both of which are more directly influenced by the inflow turbulence over the rotor plane, a larger number of inflow modes are needed to achieve the same accuracy that is possible with a few modes for the edgewise bending moment. Also, when comparing results for flapwise blade bending and fore-aft tower bending, it is seen that a greater number of POD modes are required for fore-aft tower bending. This is because, in the case of flapwise blade bending, comparatively more energy is concentrated at very low frequencies (see Fig. 15), where again a small number of inflow POD modes can accurately describe the inflow turbulence field. The first inflow POD mode alone accounts for approximately 80% and 50% of the variance, respectively, of the flapwise blade bending moment and the fore-aft tower bending moment processes. Overall, about five inflow POD modes may be sufficient to capture the variance (energy) in turbine blade bending loads, while for tower bending loads where the low-frequency energy is not as dominant, a somewhat larger number of inflow POD modes (say ten) may be required to achieve the same level of accuracy. Note that truncation of the higher inflow POD modes associated with small amounts of energy does not lead to as large errors in variance of blade bending loads as it does to variance in the inflow turbulence itself (Fig. 6). Again, this is due to the turbine's rotational sampling of the inflow field. Finally, Fig. 20 shows the ratio of POD-based mean ten-minute response extremes to the target mean ten-minute extreme. It is seen that with a single POD mode, turbine load extremes are within 20% of the target levels for each of the three cases. Note that the convergence rate for edgewise blade bending moment extremes is actually slower than that for the other two response measures. This is possibly due to the highly non-Gaussian character of the edgewise blade bending process. Even though reduced-order POD representations can be accurate for edgewise bending loads variance, higher moments (such as skewness and kurtosis) important for predicting extremes need to be studied for convergence with number of inflow modes.

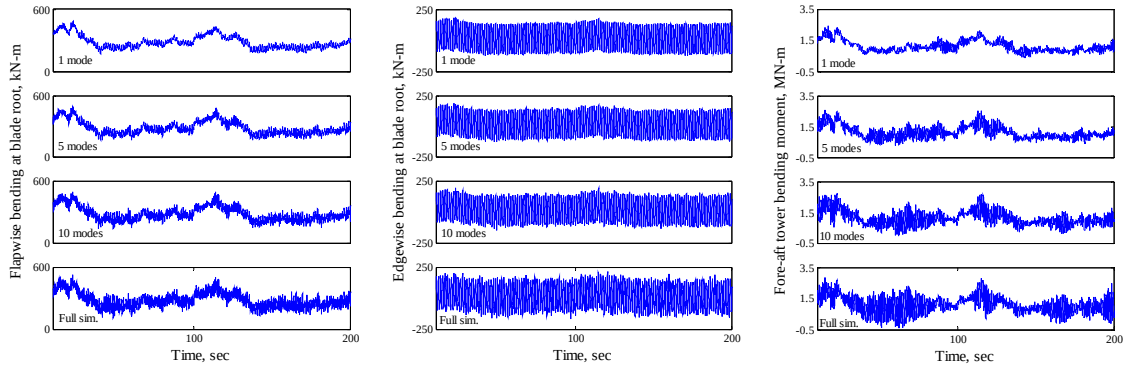

Figure 13. Plots of (a) flapwise bending moment at the blade root, (b) edgewise bending moment at the blade root, and (c) fore-aft tower base bending moment derived from 1, 5, and 10 POD inflow modes compared with full-field simulations.

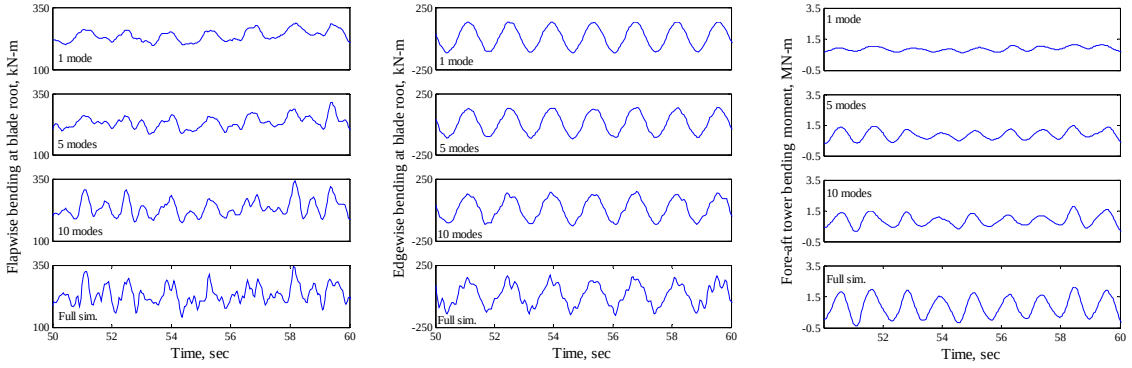

Figure 14. Zoomed-in 10-second plots of (a) flapwise bending moment at the blade root, (b) edgewise bending moment at the blade root, and (c) fore-aft tower base bending moment derived from 1, 5, and 10 POD inflow modes compared with full-field simulations.

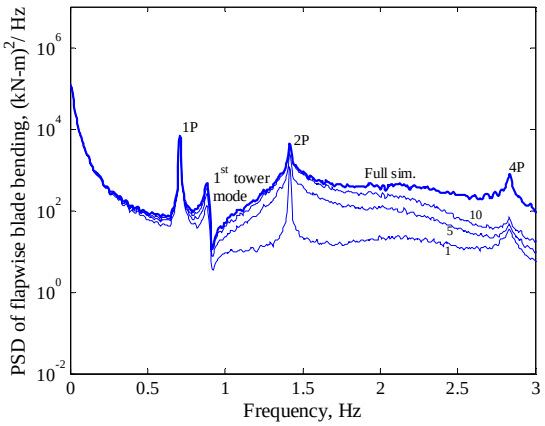

Figure 15. Contribution of 1, 5, and 10 inflow POD modes to the PSD of the flapwise bending moment at the blade root compared with the target PSD based on full-field inflow simulations.

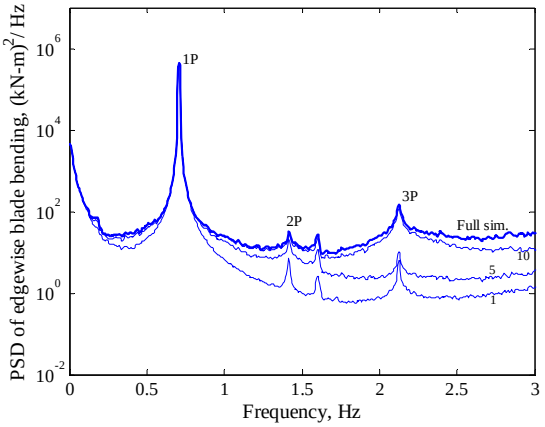

Figure 16. Contribution of 1, 5, and 10 inflow POD modes to the PSD of the edgewise bending moment at the blade root compared with the target PSD based on full-field inflow simulations.

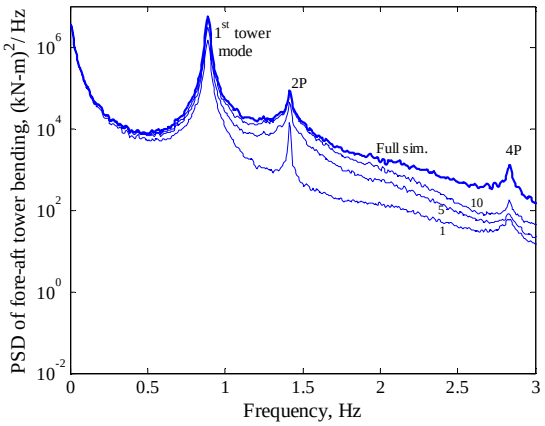

Figure 17. Contribution of 1, 5, and 10 inflow POD modes to the PSD of the fore-aft tower bending moment at the base compared with the target PSD based on full-field inflow simulations.

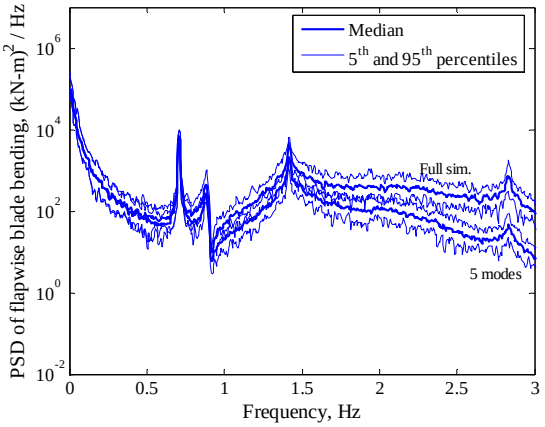

Figure 18. Median, 5th percentile, and 95th percentile PSD estimates of flapwise bending moment at the blade root using 5 POD modes compared with full-field inflow simulations.

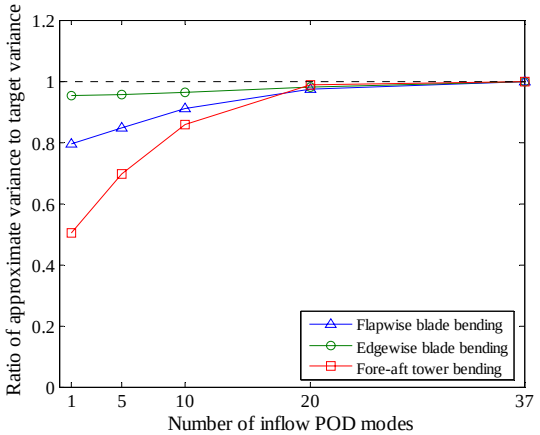

Figure 19. Ratio of variance of turbine response measures based on 1, 5, 10, 20, and 37 POD modes to the target variance.

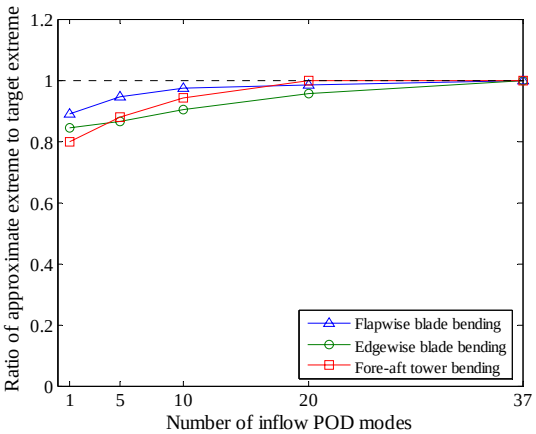

Figure 20. Ratio of ten-minute mean extreme turbine response measures based on 1, 5, 10, 20, and 37 POD modes to the target mean extreme.

C. Discussion on the effect of across-wind and vertical turbulence components on turbine response

In this study, the empirical orthogonal decomposition of the inflow turbulence random field has been carried out only for the along-wind (u) turbulence field. The across-wind (v) and vertical (w) components have not been involved in the POD analysis primarily because the IEC exponential coherence model assumes no correlation between v (or w) turbulence signals at different spatial locations. Cross-coherence between pairs of orthogonal turbulence components is also not assumed to be present. This implies that the assumed v and w turbulence fields are already in their principal components and hence there is no reason to apply the POD procedure to search for new principal bases for these two components. A different reason for not using the POD procedure with the v and w turbulence field is that these components sometimes play an insignificant role in establishing turbine design loads compared to the along-wind (u) turbulence component. For instance, for the three turbine response measures studied here, very small reduction in load statistics such as variance and extremes are seen to result when the v and w inflow turbulence components are completely ignored as seen in Table 1. For all turbine response measures, and whether comparing with the full-field simulation case or with the use of 5 POD inflow modes for the u component, errors in response variance and ten-minute mean extreme are less than 3 percent from ignoring v and w turbulence. It is important to remember, though, that these results are based on the assumption that there is no correlation of v- and w-turbulence components at different spatial locations and that there is also no correlation among the three turbulence components. Any introduction of cross-coherence among the three turbulence components (e.g., between the u- and w- components) will likely lead to some influence of turbulence components other than the along-wind component alone. The POD procedure can easily be extended to establish full three-dimensional inflow turbulence field representations in such cases.

Table 1. Estimates of variance and mean ten-minute extreme response as a percent of corresponding estimates based on full-field simulation with inclusion of across-wind (v) and vertical (w) components in the inflow.

Turbine Response Measure	Variance			Mean 10-minute extreme		
	5 POD modes for u (no v and w)	5 POD modes for u (u, v, and w)	Full-field simulation (no v and w)	5 POD modes for u (no v and w)	5 POD modes for u (u, v, and w)	Full-field simulation (no v and w)
Flapwise bending	84.6	85.0	99.6	93.2	94.5	99.6
Edgewise bending	95.2	95.5	99.8	84.1	86.4	98.9
Fore-aft tower bending	66.8	68.7	98.1	87.2	87.8	99.5

IV. Conclusion

In this study, Proper Orthogonal Decomposition (POD) techniques were employed to characterize a simulated along-wind turbulence field assumed to be experienced by a wind turbine. Different numbers of inflow POD modes were considered in low-dimensional representations of the turbulence field. It was found that a significant portion of the energy in the along-wind turbulence came from the first few POD modes. Using a small number of POD modes, the low-frequency characteristics of the simulated turbulence field could be approximated reasonably well. To achieve a good representation of the high-frequency content in the inflow turbulence, however, a larger number of POD modes was required. The contribution of different numbers of inflow POD modes of the along-wind turbulence to turbine structural response was also studied. Reconstructed wind turbulence time series over 36 grid points on the rotor plane (plus the rotor center), with several choices of number of empirical orthogonal modes, were used to perform wind turbine response simulations on the National Wind Technology Center's Advanced Research Turbine (ART) in order to illustrate how well low-dimensional representations of the inflow turbulence field could describe wind turbine loads/responses. Across-wind and vertical turbulence components were included in the inflow simulations but no POD analyses were required for these turbulence components based on the assumed coherence models. Results suggest that the low-frequency energy in each turbine response measure was represented reasonably well by the inclusion of only a small number of inflow POD modes. Truncation of the higher inflow POD modes associated with small amounts of energy did not reduce the turbine response variance significantly as long as the energy of the turbine response measure under consideration was mostly concentrated in the low-frequency region (as was the case for the edgewise bending moment at the blade root) where a small number of inflow POD modes can accurately describe the inflow turbulence field. It was also found that with only a few inflow POD modes, turbine response extremes were close to levels based on full-field inflow simulation.

Appendix

Kaimal spectral model (an approximate version, based on IEC[5] guidelines)

$$\frac{fS_1(f)}{\sigma_1^2} = \frac{4fL_1/V_{\text{hub}}}{\left(1+6fL_1/V_{\text{hub}}\right)^{5/3}} \tag{A-1}$$

where V_{hub} is the wind speed at hub-height averaged over 10 minutes;
f is the frequency in Hertz;
S_1 is the one-sided velocity component power spectrum;
σ_1 is the velocity component standard deviation;
L_1 is the velocity component integral scale parameter.

IEC Exponential coherence model[5]

$$\text{coh}(r, f) = \exp\left(-8.8\left(\left(fr/U\right)^2 + \left(0.12r/L_c\right)^2\right)^{1/2}\right) \tag{A-2}$$

where coh*(r,f)* is the coherency function (for the longitudinal velocity component) defined as the complex magnitude cross-spectral density at two spatial locations divided by the autospectrum function;
f is the frequency in Hertz;
r is the magnitude of the projection of the separation vector between the two points under consideration onto a plane normal to the average wind direction;
L_c is the coherency scale parameter.

Acknowledgments

The authors gratefully acknowledge the financial support provided by Grant No. 003658-0272-2001 through the Advanced Research Program of the Texas Higher Education Coordinating Board and by Grant No. 30914 from Sandia National Laboratories. They also acknowledge help received from Dr. Alan Wright and Dr. Maureen Hand of the National Renewable Energy Laboratory (NREL) with the wind turbine simulation models.

References

[1]Holmes, P., Lumley J. L., and Berkooz, G., *Turbulence, Coherent Structures, Dynamical Systems and Symmetry*, Cambridge Monogr. Mech., Cambridge University Press, 1996.

[2]Li, Y., and Kareem, A., "Stochastic Decomposition and Application to Probabilistic Dynamics," *Journal of Engineering Mechanics*, Vol. 121, No. 1, 1995, pp. 162-174.

[3]Carassale, L., and Solari, G., "Proper Orthogonal Decomposition of Multi-Variate Loading Processes," *Proc. 8th ASCE Joint Specialty Conference on Probabilistic Mechanics and Structural Reliability*, Notre Dame, Indiana, 2000.

[4]Spitler, J. E., Morton, S. A., Naughton, J. W., and Lindberg, W. R., "Initial Studies of Low-Order Turbulence Modeling of the Wind Turbine In-flow Environment," *Proc. of the ASME Wind Energy Symposium*, AIAA, Reno, Nevada, 2004, pp. 442-451.

[5]IEC, "Wind Turbine Generator Systems Part 1: Safety Requirements," International Electrotechnical Commission (IEC), IEC/TC 88 61400-1, 2nd ed., Geneva, 1998.

[6]Lumley, J. L., *Stochastic Tools in Turbulence*, Academic Press, New York, 1970.

[7]Chen, X., and Kareem, A., "POD in reduced order modeling of dynamic load effects," *Proc. 9th International Conference on Applications of Statistics and Probability in Civil Engineering (ICASP9)*, Vol. 2, San Francisco, California, 2003, pp. 1591-1598.

[8]Snow, A. L., Heberling, C. F. II, and Van Bibber, L. E., "The Dynamic Response of a Westinghouse 600-kW Wind Turbine," Rept. SERI/STR-217-3405, Solar Research Institute, 1989.

[9]Veers, P. S., "Three-dimensional Wind Simulation," Sandia National Laboratory, Rept. SAND 88-0512, Albuquerque, New Mexico, 1988.

[10]Buhl, M.L. Jr., "SNwind User' Guide," National Renewable Energy Laboratory, Golden, Colorado, 2003.

[11]Saranyasoontorn, K., Manuel, L., and Veers, P. S., "A Comparison of Standard Coherence Models for Inflow Turbulence with Estimates from Field Measurements," *Journal of Solar Energy Engineering*, (to be published).

[12]Saranyasoontorn, K., and Manuel, L., "On Estimation of Empirical Orthogonal Modes in Inflow Turbulence for Wind Turbines," *Proc. 9th ASCE Joint Specialty Conference on Probabilistic Mechanics and Structural Reliability*, Albuquerque, New Mexico, 2004.

[13]Davenport, A. G., "The Spectrum of Horizontal Gustiness near the Ground in High Winds," *Quart. J. Roy. Met. Soc.*, Vol. 87, 1961, pp. 194-211.

[14]Jonkman, J. M., and Buhl, M. L. Jr., "FAST User's Guide," National Renewable Energy Laboratory, Rept. NREL/EL-500-29798, Golden, Colorado, 2004.